Non-Double-Couple Components of the Moment Tensor in a Transversely Isotropic Medium

William Menke*[1] and Joshua B. Russell[1]

ABSTRACT

The non-double-couple (non-DC) components of the moment tensor provide insight into the earthquake processes and anisotropy of the near-source region. We investigate the behavior of the isotropic (ISO) and compensated linear vector dipole (CLVD) components of the moment tensor for shear faulting in a transversely ISO medium with an arbitrarily oriented symmetry axis. Analytic formulas for ISO and CLVD depend on the orientation of the fault relative to the anisotropy symmetry axis as well as three anisotropic parameters, which describe deviations of the medium from isotropy. Numerical experiments are presented for the preliminary reference Earth model. Both ISO and CLVD components are zero when the axis of symmetry is within the fault plane or the auxiliary plane. For any orientation in which the ISO component is zero, the CLVD component is also zero, but the opposite is not always true (e.g., for strong anisotropy). The relative signs of the non-DC components of neighboring earthquakes may help distinguish source processes from source-region anisotropy. We prove that an inversion of ISO and CLVD components of a set of earthquakes with different focal mechanisms can uniquely determine the orientation and strength of anisotropy. This study highlights the importance of the ISO component for constraining deep slab anisotropy and demonstrates that it cannot be neglected.

KEY POINTS

- Non-double-couple moment tensor components of a fault in transverse isotropic medium are derived analytically.
- All non-double-couple components are zero when the symmetry axis of the anisotropy is within the fault plane.
- The explosive and compensated linear vector dipole components uniquely determine the deviation from isotropy.

Supplemental Material

INTRODUCTION

Shear faulting in a homogeneous isotropic (ISO) medium is described by the double-couple (DC) model with no volume change (Burridge and Knopoff, 1964). In reality, moment tensors often comprise additional non-DC components including an ISO (or "explosive-implosive") term and a so-called compensated linear vector dipole (CLVD). Such departures from pure DC behavior are commonly observed in earthquake catalogs, including the Global Centroid Moment Tensor (CMT) catalog, where a nonzero CLVD is routinely observed but the ISO component is constrained to be zero (Ekström *et al.*, 2012). One class of explanations attributes these components to the earthquake source itself, including tensile faulting (Robson *et al.*, 1968; Ross *et al.*, 1996; Vavryčuk, 2001, 2002, 2011); fluid injection (Kanamori *et al.*, 1993), complex rupture dynamics involving two or more subfaults (Kuge and Kawakatsu, 1993; Frohlich, 1994); and transformational faulting due to a phase transition (Vaišnys and Pilbeam, 1976; Kirby, 1987; Kirby *et al.*, 1991; Wiens *et al.*, 1993; Green and Houston, 1995). A second class of explanations attributes them to elastic anisotropy in the source region (Kawasaki and Tanimoto, 1981; Julian *et al.*, 1998; Vavryčuk, 2004, 2005; Vavryčuk *et al.*, 2008; Li *et al.*, 2018). We focus here on this case.

Starting in the 1960s, elastic anisotropy of earth materials has been intensively studied in many contexts (Anderson, 1961; see also Kawakatsu, 2016a,b); its fundamental properties are described in many texts (e.g., Love, 1927; Nye, 1985; Aki and Richards, 2009). Anisotropy due to the lattice preferred orientation (LPO) of olivine has been observed in the oceanic lithosphere (Hess, 1964; Morris *et al.*, 1969; Raitt *et al.*, 1969; Nishimura and Forsyth, 1989; Ekström and Dziewonski, 1998; Lin *et al.*, 2016; Russell *et al.*, 2019) and deeper mantle (Anderson and Dziewonski, 1982; Ekström and Dziewonski,

1. Lamont-Doherty Earth Observatory of Columbia University, Palisades, New York, U.S.A.

*Corresponding author: menke@ldeo.columbia.edu

Cite this article as Menke, W., and J. B. Russell (2020). Non-Double-Couple Components of the Moment Tensor in a Transversely Isotropic Medium, *Bull. Seismol. Soc. Am.* **XX**, 1–9, doi: 10.1785/0120190319

1998; Nettles and Dziewonski, 2008, French and Romanowicz, 2014; Moulik and Ekström, 2014; Eddy *et al.*, 2019). Because seismic anisotropy is ubiquitous, some earthquakes can occur in an anisotropic source zone.

Our understanding of earthquake source processes and crust and mantle anisotropy are intimately linked through the non-DC components of the moment tensor. As Vavryčuk (2004) has shown, these components are easily calculated, given a fault with a particular orientation and a medium described by an anisotropic elastic tensor with orthorhombic symmetry (i.e., 12 independent parameters). Here, we build upon this previous framework by considering a higher symmetry form of anisotropy—transverse isotropy (TI)—that is fully described by only seven parameters and is commonly invoked in the seismological literature. The relatively simple, yet seismically relevant, TI system offers insight into the otherwise complex relationships between the non-DC components of the moment tensor. Although we focus here on TI media, the general methodology that we employ extends also to lower symmetry systems of anisotropy (e.g., orthorhombic).

In this article, we treat shear faulting in a TI medium and systematically explore variation of the ISO and CLVD components of the moment tensor with varying fault orientations. Although TI is simple, it has proved extremely powerful in describing average Earth materials and has been invoked in many studies of mantle anisotropy (e.g., Backus, 1965; Dziewonski and Anderson, 1981; Montagner and Tanimoto, 1991; Gu *et al.*, 2005; Nettles and Dziewonski, 2008; Beghein *et al.*, 2014; Moulik and Ekström, 2014). We first derive analytical solutions for both ISO and CLVD components of the moment tensor for varying fault geometry. Second, we present numerical calculations for an arbitrarily oriented fault in the real Earth and demonstrate the importance of accounting for both non-DC components when inferring anisotropy strength and orientation.

METHODS

The intensity of ISO and CLVD components are controlled by the relative orientation of the anisotropic material and the fault. This orientation is described by two Euler angles because the medium is rotationally invariant about the TI symmetry axis. In our approach, we fix the orientation of anisotropic material and vary the orientation of the fault.

We assume a TI medium with a symmetry axis (a axis) in the vertical direction. Such a medium is conventionally parameterized with five "Love constants" A, C, F, L, and N (e.g., Dziewonski and Anderson, 1981; Nye, 1985; Nettles and Dziewonski, 2008). A sixth parameter η is sometimes used to quantify the ratio $\eta = F/(A-2L)$. In the ISO case, $A = C = \lambda + 2\mu$, $L = N = \mu$, $F = \lambda$, and $\eta = 1$, in which λ and μ are the Lamé parameters. The elastic tensor c_{ijpq} can be formed from the Love constants, starting with $c_{1111} = c_{2222} = A$, $c_{3333} = C$, $c_{1313} = c_{2323} = L$, $c_{1212} = N$, $c_{1122} = A - 2N$, and $c_{1133} = c_{2233} = F$ (Musgrave, 1970; Aki and Richards, 2009). The strength of anisotropy can be quantified by possibly large deviations ΔC, ΔN, and ΔF, with $C \equiv A + \Delta C$, $N \equiv L + \Delta N$, and $F \equiv (A - 2N) + \Delta F$. The medium is ISO if $\Delta C = \Delta N = \Delta F = 0$.

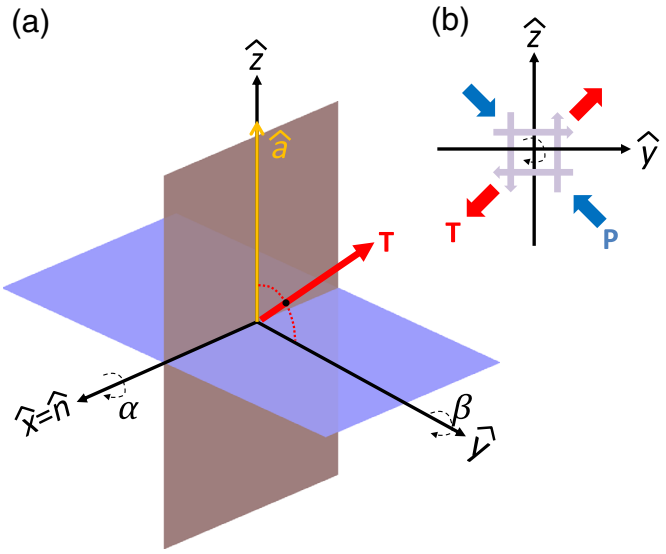

Figure 1. (a) Geometry of the fault plane (vertical) and auxiliary plane (horizontal). The two planes intersect along the null axis $\hat{n}$. The axis of transverse isotropy (TI) $\hat{a}$ is initially within the fault plane and perpendicular to the null axis. A rotation of the fault by an angle α about the x axis moves the axis $\hat{a}$ of TI (arrow parallel to $\hat{z}$) off the fault plane. A rotation of the fault by an angle β about the y axis keeps the $\hat{a}$ axis within the fault plane.
(b) Simplified sketch showing the (x, z) plane and highlighting the fault-slip directions (thin arrows) and the P and T axes (arrows labeled P and T). The color version of this figure is available only in the electronic edition.

In the reference orientation, the fault lies in the vertical (x, z) plane and the slip is in the x direction (Fig. 1). Consequently, the fault-plane normal is $\mathbf{v} = [0 \quad 1 \quad 0]^{\mathrm{T}}$ and the slip direction is $\mathbf{u} = [1 \quad 0 \quad 0]^{\mathrm{T}}$. The T, P, and B axes are parallel to $(\mathbf{u} + \mathbf{v})$, $(\mathbf{u} - \mathbf{v})$, and $\mathbf{w} \equiv \mathbf{u} \times \mathbf{v}$, respectively. The plane defined by reversing the roles $\mathbf{u}$ and $\mathbf{v}$ is conventionally called the "auxiliary" plane. We refer to the plane containing the P and T axes as the "equatorial plane" and the plane containing the P and B axes as the "meridional" plane. The rupture on the fault can be described by the fault tensor $F^{(0)}_{pq} \equiv (u_p v_q + u_q v_p)$ (Vavryčuk, 2004; Aki and Richards, 2009). It can be shown that vectors parallel to the T, P, and B axes are eigenvectors of $\mathbf{F}^{(0)}$, with eigenvalues of $\lambda^{(1)} = 1$, $\lambda^{(2)} = -1$, and $\lambda^{(3)} = 0$, respectively. Consequently, $\det(\mathbf{F}^{(0)}) = \lambda^{(1)}\lambda^{(2)}\lambda^{(3)} = 0$. The fault is rotated into other orientations by applying a rotation matrix $\mathbf{R}$, that is, $F_{pq} = R_{pi}R_{qj}F^{(0)}_{ij}$ (in which summation over repeated indexes is implied).

The moment tensor $\mathbf{M}$ equivalent to the fault is $M_{ij} = \bar{u}\Omega m_{ij}$ with $m_{ij} \equiv c_{ijpq}F_{pq}$, in which $\bar{u}$ is the average slip on the fault and Ω is the fault area (Aki and Richards, 2009). The relative sizes of components depend only on $\mathbf{m}$ and not on

the multiplicative factor of $\bar{u}\Omega$ (which can be set to unity). A purely ISO moment tensor is diagonal, $\mathbf{m} = X\mathbf{I}$, in which $\mathbf{I}$ is the identity matrix (Aki and Richards, 2009). The amplitude X is negative for an implosion and positive for an explosion. The amplitude X associated with an arbitrary moment tensor is $X \equiv \mathrm{tr}(\mathbf{m})$. The deviatoric part of the moment tensor, $\Delta\mathbf{m} = \mathbf{m} - \mathrm{tr}(\mathbf{m})\mathbf{I}$, has zero trace. The CLVD is defined by eigenvalues $-\frac{1}{2}\lambda^{(p)} = -\frac{1}{2}\lambda^{(q)} = \lambda^{(r)}$, in which (p, q, r) are permutations of (1,2,3) (Frohlich, 1994; Vavryčuk, 2015). The eigenvector $v^{(r)}$ associated with $\lambda^{(r)}$ is the axis of symmetry of the CLVD. When it is positive, we will refer to the CLVD as "dilatational along its axis," and when it is negative, we will refer to it as "compressional along its axis." The smallest CVLD that can be subtracted from $\Delta\mathbf{m}$ to produce one identically zero eigenvalue is $-\frac{1}{2}\lambda^{(p)} = -\frac{1}{2}\lambda^{(q)} = \lambda^{(r)} = \lambda^{(\min)}$, in which $\lambda^{(\min)}$ is the eigenvalue with the smallest absolute value. Consequently, the amplitude V of the CLVD component is quantified by $V \equiv \lambda^{(p)}$ with $p = \mathrm{argmin}_i|\lambda^{(i)}|$.

We derive the fault matrix $\mathbf{F}(\beta)$ by analytically rotating the fault by angle β and derive the moment tensor $\mathbf{m}(\beta)$ by analytically contracting the fault tensor with the elastic tensor. We then derive amplitudes $X(\beta)$ and $V(\beta)$ of the ISO and CLVD components, respectively, by analytically solving the cubic discriminant equation. All derivations have been verified through a comparison with numerical calculations and are presented in the supplemental material to this article.

RESULTS

Property 1. The ISO component is zero when the TI symmetry axis is within the fault plane. Rotating the reference fault by angle β about the y axis keeps the TI symmetry axis within the fault plane. Defining $c \equiv \cos\beta$ and $s \equiv \sin\beta$, the moment tensor is found to be

$$\mathbf{F}(\beta) = \begin{bmatrix} 0 & s & 0 \\ s & 0 & c \\ 0 & c & 0 \end{bmatrix} \quad \text{and} \quad \mathbf{m}(\beta) = \begin{bmatrix} 0 & 2sN & 0 \\ 2sN & 0 & 2cL \\ 0 & 2cL & 0 \end{bmatrix}. \tag{1a, b}$$

The diagonal elements of $\mathbf{m}(\beta)$ are all zero, implying that $X(\beta) = 0$ for all β.

Property 2. The CLVD component is zero when the TI symmetry axis is within the fault plane. Because the diagonal elements of $\Delta\mathbf{m}(\beta)$ are identically zero, its determinant is zero for all β. Consequently, it must have at least one zero eigenvalue and $V(\beta) = 0$ for all β.

Property 3. The ISO component is $X(\alpha) = -(\Delta F + \Delta C)\sin 2\alpha$ when the TI symmetry axis is within the equatorial plane. Rotating the reference fault by angle α about the x axis keeps the TI symmetry axis in the equatorial plane and aligns the P axis with the a axis when $\alpha = \pi/4$:

$$\mathbf{F}(\alpha) = \begin{bmatrix} 0 & 0 & 0 \\ 0 & \sin 2\alpha & \cos 2\alpha \\ 0 & \cos 2\alpha & -\sin 2\alpha \end{bmatrix}$$

$$\mathbf{m}(\alpha) = \begin{bmatrix} -\Delta F \sin 2\alpha & 0 & 0 \\ 0 & (2L + 2\Delta N - \Delta F)\sin 2\alpha & 2L\cos 2\alpha \\ 0 & 2L\cos 2\alpha & (-2L - 2\Delta N + \Delta F - \Delta C)\sin 2\alpha \end{bmatrix}. \tag{2a, b}$$

The ISO component is calculated as $\mathrm{tr}(\mathbf{m}) = -(\Delta F + \Delta C)\sin 2\alpha$.

Property 4. For weak anisotropy, the CLVD component is $V(\alpha) = -(\Delta C - 2\Delta F)\sin 2\alpha$ when the TI symmetry axis is within the equatorial plane (but can depart significantly from this value for strong anisotropy). The discriminant $\det(\Delta\mathbf{m}(\alpha) - \lambda) = 0$ has roots:

$$\begin{aligned} 2\lambda^{(1)} &= -g + [g^2 - 4h]^{1/2} \\ 2\lambda^{(2)} &= -g - [g^2 - 4h]^{1/2} \\ \lambda^{(3)} &= \frac{1}{3}(\Delta C - 2\Delta F)\sin 2\alpha, \end{aligned} \tag{3}$$

with

$$g \equiv \frac{1}{3}(\Delta C - 2\Delta F)\sin 2\alpha$$

$$g^2 - 4h \equiv (4L + 4\Delta N - 2\Delta F + \Delta C)^2 \sin^2 2\alpha + 16L^2 \cos^2 2\alpha. \tag{4}$$

In the isotropic limit, in which $(\Delta C, \Delta F, \Delta N) \to 0$, we find $\lambda^{(1)} \to 2L$, $\lambda^{(2)} \to -2L$, and $\lambda^{(3)} \to 0$. Hence, for weak anisotropy, $\lambda^{(3)}$ is the eigenvalue with the smallest absolute value, $V = \lambda^{(3)}$ and V varies sinusoidally along the equator, attaining the extreme value of $(\Delta C - 2\Delta F)$ at $\alpha = \pi/4$. In this case, the ratio $R = V/X = (2\Delta F/\Delta C - 1)/(\Delta F/\Delta C + 1)$ depends only on the ratio $\Delta F/\Delta C$ and is constant along the equator. For arbitrary anisotropy, but for $\alpha = \pi/4$, we find that

$$\begin{bmatrix} \lambda^{(1)} \\ \lambda^{(2)} \\ \lambda^{(3)} \end{bmatrix} = \begin{bmatrix} (2\Delta C - \Delta F) + |4L + 4\Delta N - 2\Delta F + \Delta C|^2 \\ (2\Delta C - \Delta F) - |4L + 4\Delta N - 2\Delta F + \Delta C|^2 \\ (\Delta C - 2\Delta F) \end{bmatrix}. \tag{5}$$

Depending upon the values of the Love constants and the magnitude of anisotropy, either $\lambda^{(1)}$ or $\lambda^{(2)}$ may have an absolute

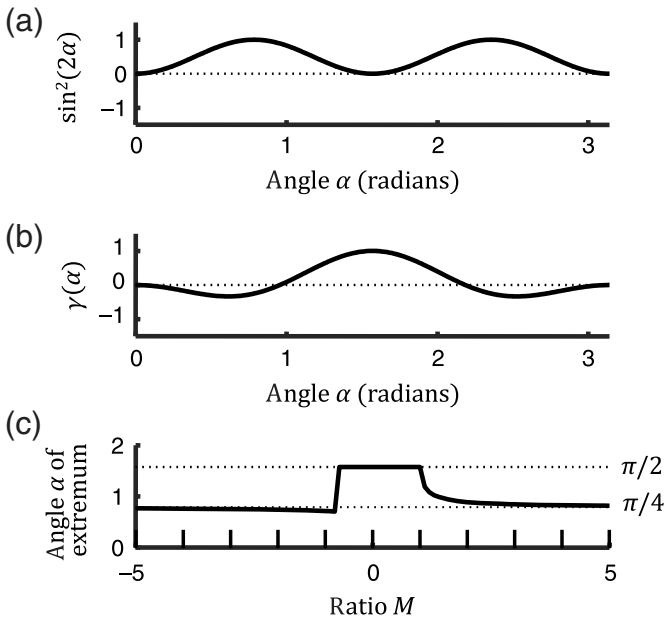

Figure 2. (a) The function at $\sin^2(2\alpha)$ as a function of angle α. (b) The function at $\gamma(\alpha)$ as a function of angle α. (c) The angle at which $M\sin^2(2\alpha) + \gamma(\alpha)$ attains its extreme value, as a function of M. See the Results section for further discussion.

value that is smaller than $|\lambda^{(3)}|$. When this "eigenvalue switching" occurs, V will equal that eigenvalue. Irrespective of anisotropy strength, $\lambda^{(3)}$ is the eigenvalue with the smallest absolute value when the rotation angle α is small (that is, the fault plane is close to $\hat{\mathbf{x}}$). Therefore, in the limit $\alpha \to 0$, $R = (2\Delta F/\Delta C - 1)/(\Delta F/\Delta C + 1)$. Furthermore, this is the extreme value of R because the switch to a different eigenvalue only occurs when the absolute value of that eigenvalue is closer to zero, that is, $|V|$ decreases.

Property 5. The ISO component is $X = -(\Delta F + \Delta C)\sin^2\alpha$ when the TI symmetry axis is within the meridional plane. We first orient the reference fault such that the meridional plane aligns with the (y, z) plane. We then rotate it by an angle α about the x axis, which keeps the a axis aligned with the meridional plane. Defining $c \equiv \cos\alpha$ and $s \equiv \sin\alpha$, we get

$$\mathbf{F}(\alpha) = \begin{bmatrix} 1 & 0 & 0 \\ 0 & -c^2 & cs \\ 0 & cs & -s^2 \end{bmatrix}, \tag{6}$$

Property 6. When anisotropy is weak and the TI symmetry axis is within the meridional plane, the CLVD component is

$$V = -\Delta N \sin^2 2\alpha + \frac{1}{3}(\Delta F + 2\Delta C)\gamma(\alpha)$$
$$\text{with } \gamma(\alpha) \equiv \left(-\frac{3}{2}\right)\left\{\left(\frac{1}{6}\right) + \left(\frac{2}{6}\right)\cos 2\alpha - \left(\frac{3}{6}\right)\cos^2 2\alpha\right\}. \tag{8}$$

This result is achieved in the following steps: first, the cubic discriminant is calculated as $\det(\Delta\mathbf{m}(\alpha) - \lambda) = 0$; second, one solution is identified as $\lambda^{(1)} = \Delta m_{11}$, allowing for the identification of the quadratic equation solved by $\lambda^{(2)}$ and $\lambda^{(3)}$; third, the quadratic equation is solved; and fourth, the square root in the expressions for the smallest eigenvalue, say $\lambda^{(3)}$, is expanded in a Taylor series to allow for the cancelation of zero-order terms and to achieve a result that depends only upon Love constant deviations.

For weak anisotropy, $V(\alpha)$ is a linear combination of two functions, $\sin^2 2\alpha$ (Fig. 2a) and $\gamma(\alpha)$ (Fig. 2b). Using the ratio $M \equiv 3\Delta N/(\Delta C - 2\Delta F)$ as a measure of the relative size of the two terms, we find that for weak anisotropy and $|M| \gg 1$, $V(\alpha)$ attains its extreme value at $a = \pi/4$ (at which point $\sin^2 2\alpha = -1$). Also, for weak anisotropy, but for $|M| \ll 1$, $V(\alpha)$ attains its extreme value at $\alpha = \pi/2$ (at which point $\gamma = 1$). For intermediate values of $|M|$, the location of the extreme value varies as is shown in Figure 2c.

As $\alpha \to 0$, both V and X vary as α^2. Consequently, the ratio $R = V/X$ is, in the limit, a nonzero constant:

$$R = \frac{-4\Delta N + (4/3)(\Delta F - \tfrac{1}{2}\Delta C) + 2L^{-1}(\Delta N)^2}{-\frac{1}{3}(\Delta F + \Delta C)} + O(L^{-2}). \tag{9}$$

Property 7. For a general rotation described by angles (θ, φ), the amplitude of ISO is $X(\theta, \varphi) = -(\Delta F + \Delta C)\cos(2\theta)\sin(\varphi)$. Starting with the fault in its principal coordinate system (as in property 5), we rotate the fault tensor by an angle of θ about the z axis, followed by an angle of φ about the new x axis. We then analytically evaluate $\mathrm{tr}(\mathbf{m}) = c_{ppij}F_{ij}$. The algebra is simplified by writing $c_{ppij} = c^{(0)}_{ppij} + c^{(1)}_{ppij}$, in which $c^{(0)}_{ppij}$ depends only upon the Love constants and $c^{(1)}_{ppij}$ depends only upon their deviations. Then, $\mathrm{tr}(\mathbf{m}) = c^{(1)}_{ppij}F_{ij}$ because $c^{(0)}_{ppij}F_{ij} = 0$. The ISO component $X(\theta, \varphi)$ depends only upon ΔF and ΔC but not upon ΔN and is identically zero when $\Delta F + \Delta C = 0$.

$$\mathbf{m}(\alpha) = \begin{bmatrix} 2L + 2\Delta N - \Delta F s^2 & 0 & 0 \\ 0 & -2Lc^2 - 2\Delta N c^2 - \Delta F s^2 & 2Lcs \\ 0 & 2Lcs & -2Ls^2 - 2\Delta N s^2 + \Delta F s^2 - \Delta C s^2 \end{bmatrix}. \tag{7}$$

The ISO component reads $\mathrm{tr}(\mathbf{m}) = -(\Delta F + \Delta C)s^2$.

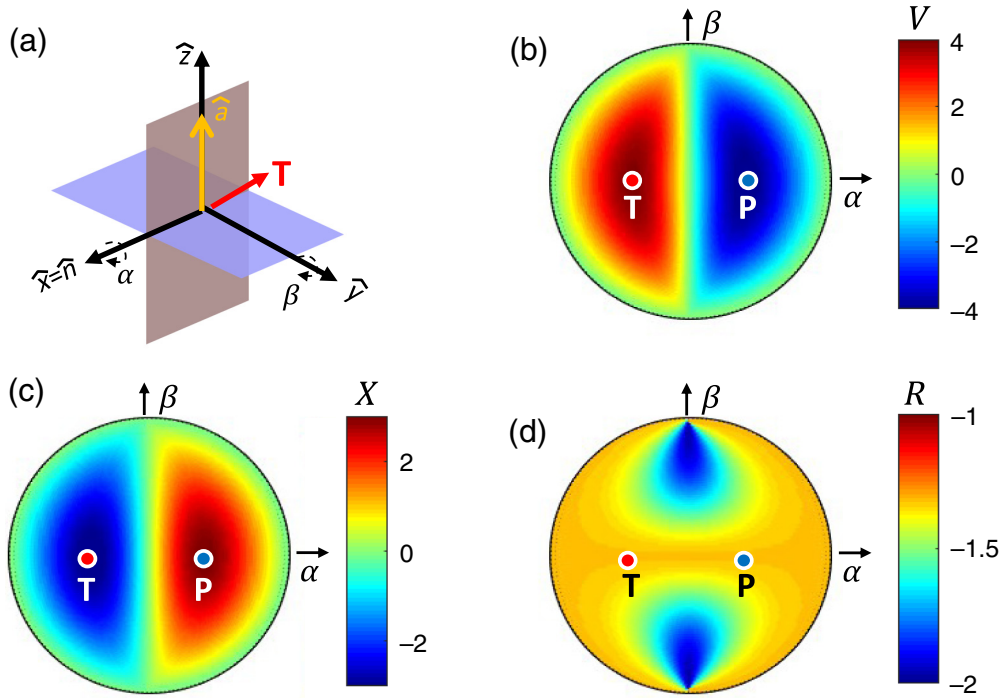

Figure 3. Results for the weak anisotropy case ($f = 1$). (a) The fault plane is initially vertical, the auxiliary plane is initially horizontal, and the n axis $\hat{n}$ is initially parallel to the x axis. The fault is tilted from the vertical by a rotation β around the y axis and a rotation α around the x axis. Note that for $\alpha = 0$, rotations around β leave the n axis in the fault plane. (b) Stereographic plot of the strength V of the compensated linear vector dipole component. (c) The strength X of the isotropic (ISO) component. (d) The ratio, $R = V/X$. See the Results section for further discussion. The (α, β) that rotates the T axis (P axis) into alignment with the axis of TI is marked with circles. The absolute maximum element of the moment tensor is ~120, so the X and V components contribute about 2% and 4% of the total moment, respectively. The color version of this figure is available only in the electronic edition.

Example. Our example starts with a TI medium from the Dziewonski and Anderson (1981) preliminary reference Earth model (PREM), evaluated at 100 km depth and for a reference frequency of 1 Hz. The PREM has the following constants: $v_{pV}^{\mathrm{PREM}} = 7.94$ km/s, $v_{pH}^{\mathrm{PREM}} = 8.14$ km/s, $v_{sV}^{\mathrm{PREM}} = 4.41$ km/s, $v_{sH}^{\mathrm{PREM}} = 4.54$ km/s, $\eta^{\mathrm{PREM}} = 0.93$, and $\rho^{\mathrm{PREM}} = 3373$ kg/m^3. This model is characterized by about 2.3% P-wave anisotropy and represents a weak anisotropy case. The positive value of $-(\Delta F + \Delta C) \approx 3.0$ implies that X is positive (explosive) when the T axis aligns with the TI symmetry axis. Its low value of $|M| \approx 0.8$ implies that the extreme values of V will occur near the P and T axes.

For angles (α, β), we rotate the fault tensor $\mathbf{F}_0$. Then, we compute the moment tensor $\mathbf{m}$, its trace, the absolute smallest eigenvalue of $\Delta\mathbf{m}$, and the ratio R (Figs. 3 and 4). Both the overall behavior of V, X, and R and their numerical values are observed to follow the predictions of the analytic formulas. In particular, $V = 0$ and $X = 0$ when the a axis is in the plane of the fault, as predicted. Furthermore, both $V(\alpha, \beta)$ and $X(\alpha, \beta)$ have a simple, sinusoidal variation in α.

We then boost the amplitude of PREM's seismic anisotropy by a factor of 10 (without changing ρ or η) to achieve a strong anisotropy case (Fig. 5). The positive value of $-(\Delta F + \Delta C) \approx 13.4$ implies that X is positive (explosive) when the T axis aligns with the TI symmetry. As in the weak anisotropy case, both $V = 0$ and $X = 0$ when the a axis is in the plane of the fault. However, although X, as in the previous case, has a sinusoidal variation in α, the behavior of V becomes more complicated. We have verified that this complex behavior is due to eigenvalue switching; for this reason, no inference can be made based on M alone. In all cases, the numerical values of quantities closely match their analytical predictions.

DISCUSSION

When earthquakes occur on a set of faults with different orientations in a homogeneous anisotropic medium, measurements of X and V can be used to determine the intensity and direction of anisotropy (Vavryčuk, 2004, 2005). This type of inversion has recently been applied to subduction-zone earthquakes (Li *et al.*, 2018), which assume a constrained form of tilted TI. The inverse problem is complex, especially for general anisotropy, because of the complicated relationship between the observed X and V and the 21 unknown elastic parameters c_{ijpq}. We focus here on a "reduced" problem of a TI inversion, with the expectation that it will provide some insight into the structure of more complicated cases.

In TI media, measurements of X and V can uniquely determine the direction of the symmetry axis and three anisotropy parameters that quantify its strength. The orientation of the a axis is detected by matching the observed angular variation of the data to the simple and highly symmetrical predicted patterns. In principal, only four earthquakes are needed to find the axis of the predicted $X(\theta, \varphi)$ pattern and to determine the linear combination $(\Delta C + \Delta F)$. These same data also are sufficient (at least for weak anisotropy) to distinguish the two $V(\theta, \varphi)$ patterns and the linear combinations ΔN and $(\Delta F + 2\Delta C)$. Consequently, only ≥4 earthquakes are required to determine ΔC, ΔF, and ΔN in an inversion that uses both X and V.

The Global CMT catalog (Ekström *et al.*, 2012) is a primary source of information on earthquake moment tensors on the

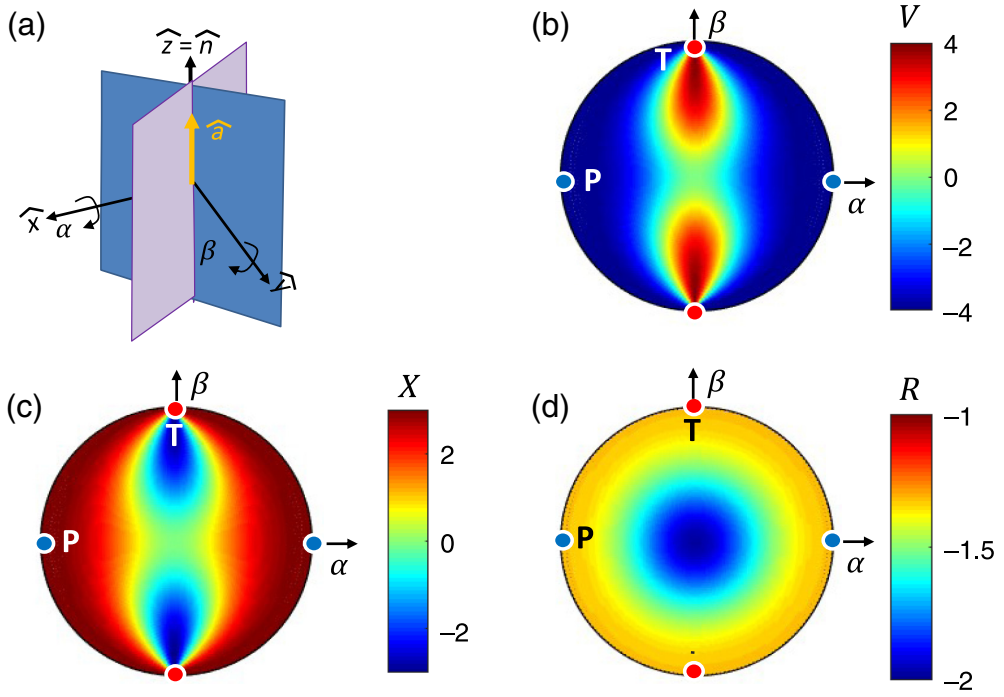

Figure 4. Same as Figure 3, except for a different reference orientation of the fault. The null axis $\hat{n}$ is initially vertical and aligned with the $\hat{a}$ axis. The x axis and y axis are 45° between the fault plane and auxiliary plane. This fault is then tilted, via a rotation β around the y axis followed by a rotation α around the x axis. See the caption of Figure 3 for further information. The color version of this figure is available only in the electronic edition.

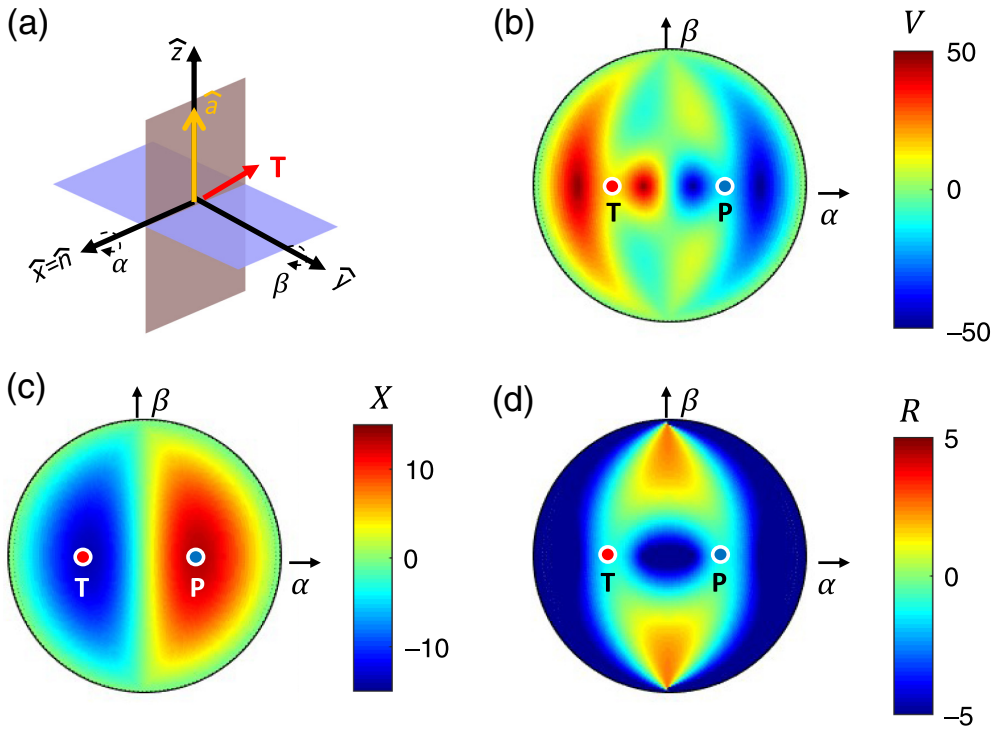

Figure 5. Same as Figure 3, except for the strong anisotropy case ($f = 10$). The absolute maximum element of the moment tensor is ~90, so the X and V components contribute about 15% and 45% of the total moment, respectively. See the Results section for further discussion. The color version of this figure is available only in the electronic edition.

global scale, although regional seismic networks can provide important measurements on smaller scales (Stierle, Bohnhoff, *et al.*, 2014; Stierle, Vavryčuk, *et al.*, 2014). However, the Global CMT provides estimates of amplitude V only. Because of poor constraints from the long-period data, X is set to zero in the inversion. The question is how to deal with the lack of information about X, but still including the prior information that they are expected to be small. One possibility is to require $X_k = 0$ for all k earthquakes, or alternatively, to seek a solution that minimizes $\sum_k X_k^2$. However, this condition is equivalent to requiring $\Delta C + \Delta F = 0$, which although mathematically sufficient to resolve the nonuniqueness, may not correspond to anisotropy common in the actual Earth; PREM, for example, does not meet this condition. However, more realistic prior information would seem to require knowledge of the mechanism by which the anisotropy is produced (e.g., by olivine LPO, thin layers, fluid-filled cracks, and so on; Fig. 6).

This study highlights the importance of accurately determining the ISO component of the moment tensor for understanding deep earthquakes. We show that, for shear faulting in a TI medium, X can be positive, negative, or zero depending on fault orientation. In contrast, phase transition hypotheses for deep earthquakes within ISO slabs predict negative (implosive) X due to volume reduction (Vaišnys and Pilbeam, 1976; Kirby, 1987; Kirby *et al.*, 1991;

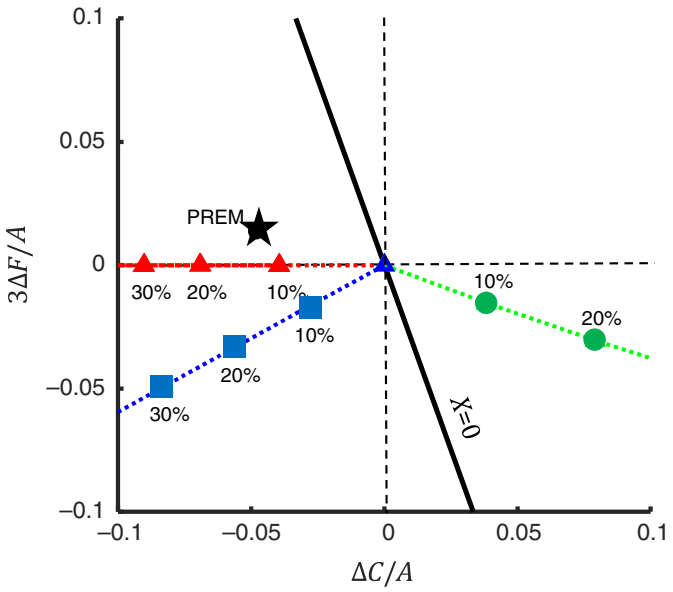

Figure 6. Four possible forms of prior information of the covariation of ΔC and ΔF: the ISO component is $X = 0$ (bold curve); the medium consists of p percent ISO olivine and $(100 - p)$ percent of a transversely ISO olivine aggregate, the fast axes of which are aligned, with the other axes randomly oriented (dotted curve with circles); the medium consists of p percent ISO olivine and $(100 - p)$ percent of a transversely ISO olivine, the slow axes of which are aligned, with the other axes randomly oriented (dotted curve with squares); and the medium consists of finely laminated ISO layers (which can mimic a transversely ISO medium) (Backus, 1962), with p percent having one velocity and $(100 - p)$ percent having another (dotted curve with triangles). Selected values of $(100 - p)$ are annotated on the curves. Preliminary reference Earth model (PREM) is shown for reference (star). The color version of this figure is available only in the electronic edition.

Wiens *et al.*, 1993; Green and Houston, 1995). However, a combination of the two mechanisms—a phase transition-induced earthquake within an anisotropic slab—could conceivably produce a net explosive mechanism. Some progress has been made in measuring X for very large earthquakes (e.g., Okal *et al.*, 2018), but more estimates from moderate-sized earthquakes will be necessary to distinguish source region anisotropy from translational faulting.

A key result is that fault orientations that lead to $X = 0$ also lead to $V = 0$, but not vice versa. This implies that X and V measurements are at least weakly correlated, which may in turn influence their statistical description. However, given that X and V depend on ΔC, ΔF, and ΔN in different ways and that this difference is greatest for high degrees of anisotropy, this correlation may be difficult to detect in real datasets.

For weak anisotropy, the patterns of variation of X and V with fault orientation are very simple. Their smooth variation with angle implies that X and V measurements from just a few earthquakes—at least four, but more realistically a few dozen—are needed to map out the pattern and hence to determine the Love constant deviations and the orientation of the axis of anisotropy. Thus, the inversion is likely to be very robust, as long as the data are not too noisy. In contrast, data that have a complicated variation with fault orientation cannot be well fitted by any weakly anisotropic model. Instead, the inversion will tend to select a strong anisotropy model because the angular pattern of V is more complex. This behavior is exactly what is desired when the data actually are caused by strong anisotropy. However, it is problematical for noisy data because the inversion will tend to fit noise by raising the strength of anisotropy. Consequently, a suitable procedure is to compare the results of the inversion with one in which the anisotropy is constrained to be weak and to test whether the improvement in fit is significant.

Although goodness-of-fit, quantified for example by the root mean square (rms) error, is a useful metric in anisotropic inversions, our findings concerning nonuniqueness indicates that, in an inversion that includes V only, a low rms error does not guarantee that the estimated anisotropy closely matches that of the Earth. Only when X and V are inverted together is the inversion unique. Because of the eigenvalue-switching behavior described earlier, the derivatives $\partial V/\partial \Delta C$, $\partial V/\partial \Delta F$, and $\partial V/\partial \Delta N$ are discontinuous and, consequently, unsuitable for use in an iterative linearized inversion based on Newton's Method. A slower but more robust inversion method, such as the Monte Carlo method used by Li *et al.* (2018), is required.

CONCLUSIONS

We study behavior of the non-DC components of the moment tensor for shear faulting in a TI medium. Analytic solutions provide insight into the relationship between source region anisotropy and the resulting non-DC components. The intensities of the ISO and CLVD components are simple functions of the parameters ΔC, ΔF, and ΔN, which describe deviations of the medium from isotropy. Both components vary in strength and sign as the fault plane is rotated with respect to the axis of symmetry of the medium. Their behaviors are summarized as follows:

1. Amplitudes X and V of the ISO and CLVD, respectively, are zero when the axis of symmetry is within the fault plane or the auxiliary plane.
2. X depends upon ΔC and ΔF through the combination $(\Delta F + \Delta C)$ but not upon ΔN. It is largest when the symmetry axis is parallel to the P or T axes and smoothly decreases away from that orientation. It is identically zero in the special case $\Delta F/\Delta C = -1$.
3. V depends upon both $(\Delta F + 2\Delta C)$ and ΔN. In some cases, it is largest when the TI symmetry axis aligns with the P or T axes, and in other cases, it is rotated by as much as 45° toward the null axis.
4. For TI anisotropy, any orientation in which X is zero, V is also zero, but the converse is not always true (e.g., strong anisotropy).

Both components alternate in sign as the fault is rotated through 360°. This behavior can help differentiate anisotropy-induced from source-induced ISO and CLVD components, that is, one would not expect both explosions and implosions in the same general area, nor CLVDs that are both compressional and dilatational along their main axes, when they are due to physical source conditions such as phase transitions, tensile crack, or fluid injections.

DATA AND RESOURCES

This article uses exemplary preliminary reference Earth model (PREM) data drawn from table 2 of Dziewonski and Anderson (1981). The transversely isotropic formulas derived in this article are special cases of the well-known general-case formulas of earthquake source mechanics in anisotropic media. Consequently, this article only provides a brief summary of the derivation method—enough to allow a mathematically inclined reader to verify the result. Full derivations are provided in the supplemental material, mostly to assist in the implementation of the formula in computer algorithms, for which details such sign conventions and choice of coordinate systems becomes very important.

ACKNOWLEDGMENTS

The authors thank the 2018 Columbia University Seismology-Geology-Tectonophysics (SGT) reading seminar for useful discussions. J. B. Russell gratefully acknowledges National Science Foundation (NSF) Graduate Research Fellowship (DGE-16-44869). This research was supported by the NSF's EarthScope, Geophysics, Ocean Science Education programs under Awards EAR11-47742, EAR-1345143, OCE13-59194, EAR-1614066, and Cooperative Agreement EAR-1261681.

REFERENCES

Aki, K., and P. G. Richards (2009). *Quantitative Seismology: Theory and Methods*, Second Ed., University Science Books, Herndon, Virginia, 732 pp., ISBN: 978-1-891389-63-4.

Anderson, D. L. (1961). Elastic wave propagation in layered anisotropic media, *J. Geophys. Res.* **66,** 2953–2963, doi: 10.1029/JZ066i009p02953.

Anderson, D. L., and A. M. Dziewonski (1982). Upper mantle anisotropy: Evidence from free oscillations, *Geophys. J. Roy. Astron. Soc.* **69,** 383–404, doi: 10.1111/j.1365-246X.1982.tb04956.x.

Backus, G. E. (1962). Long-wave elastic anisotropy produced by horizontal layering, *J. Geophys. Res.* **67,** 4427–4440, doi: 10.1029/JZ067i011p04427.

Backus, G. E. (1965). Possible form of seismic anisotropy of the upper mantle under the oceans, *J. Geophys. Res.* **70,** 3429–3439, doi: 10.1029/JZ070i014p03429.

Beghein, C., K. Yuan, N. Schmerr, and Z. Xing (2014). Changes in seismic anisotropy shed light on the nature of the Gutenberg discontinuity, *Science* **343,** 1237–1240, doi: 10.1126/science.1246724.

Burridge, R., and L. Knopoff (1964). Body force equivalents for seismic dislocations, *Seismol. Soc. Am. Bull.* **54,** 1875–1888.

Dziewonski, A. M., and D. L. Anderson (1981). Preliminary reference Earth model, *Phys. Earth Planet. In.* **25,** 297–356, doi: 10.1016/0031-9201(81)90046-7.

Eddy, C. L., G. Ekström, M. Nettles, and J. B. Gaherty (2019). Age dependence and anisotropy of surface-wave phase velocities in the Pacific, *Geophys. J. Int.* **216,** 640–658, doi: 10.1093/gji/ggy438.

Ekström, G., and A. M. Dziewonski (1998). The unique anisotropy of the Pacific upper mantle, *Nature* **394,** 168–172, doi: 10.1038/28148.

Ekström, G., M. Nettles, and A. M. Dziewonski (2012). The global CMT project 2004–2010: Centroid-moment tensors for 13,017 earthquakes, *Phys. Earth Planet. In.* **200,** 1–9, doi: 10.1016/j.pepi.2012.04.002.

French, S. W., and B. A. Romanowicz (2014). Whole-mantle radially anisotropic shear velocity structure from spectral-element waveform-tomography, *Geophys. J. Int.* **199,** 1303–1327, doi: 10.1093/gji/ggu334.

Frohlich, C. (1994). Earthquakes with non-double-couple mechanisms, *Science* **264,** 804–809, doi: 10.1126/science.264.5160.804.

Green, H. W., and H. Houston (1995). The mechanics of deep earthquakes, *Annu. Rev. Earth Planet. Sci.* **23,** 169–213, doi: 10.1146/annurev.ea.23.050195.001125.

Gu, Y. J., A. L. Lerner-Lam, A. M. Dziewoński, and G. Ekström (2005). Deep structure and seismic anisotropy beneath the East Pacific Rise, *Earth Planet. Sci. Lett.* **232,** 259–272, doi: 10.1016/j.epsl.2005.01.019.

Hess, H. (1964). Seismic anisotropy of the uppermost mantle under oceans, *Nature* **203,** 629–631, doi: 10.1038/203629a0.

Julian, B. R., A. D. Miller, and G. R. Foulger (1998). Non-double-couple earthquakes: 1. Theory, *Rev. Geophys.* **36,** 525–549, doi: 10.1029/98RG00716.

Kanamori, H., G. Ekström, A. M. Dziewonski, J. S. Barker, and S. A. Sipkin (1993). Seismic radiation by magma injection: An anomalous seismic event near Tori Shima, Japan, *J. Geophys. Res.* **98,** 6511–6522, doi: 10.1029/92JB02867.

Kawakatsu, H. (2016a). A new fifth parameter for transverse isotropy, *Geophys. J. Int.* **204,** 682–685, doi: 10.1093/gji/ggv479.

Kawakatsu, H. (2016b). A new fifth parameter for transverse isotropy II: Partial derivatives, *Geophys. J. Int.* **206,** 360–367, doi: 10.1093/gji/ggw152.

Kawasaki, I., and T. Tanimoto (1981). Radiation patterns of body waves due to the seismic dislocation occurring in an anisotropic source medium, *Seismol. Soc. Am. Bull.* **71,** 37–50.

Kirby, S. H. (1987). Localized polymorphic phase transformation in high-pressure faults and applications to the physical mechanism of deep focus earthquakes, *J. Geophys. Res.* **92,** 789–800, doi: 10.1029/JB092iB13p13789.

Kirby, S. H., W. B. Durham, and L. Stern (1991). Mantle phase changes and deep earthquake faulting in subducting lithosphere, *Science* **252,** 216–225, doi: 10.1126/science.252.5003.216.

Kuge, K., and H. Kawakatsu (1993). Significance of non-double couple components of deep and intermediate-depth earthquakes: Implications from moment tensor inversions of long-period seismic waves, *Phys. Earth Planet. In.* **75,** 243–266, doi: 10.1016/0031-9201(93)90004-S.

Li, J., Y. Zheng, L. Tomsen, T. J. Lapen, and X. Fang (2018). Deep earthquakes in subducting slabs hosted in highly anisotropic rock fabric, *Nature Geosci.* **11,** 696–700, doi: 10.1038/s41561-018-0188-3.

Lin, P.-Y. P., J. B. Gaherty, G. Jin, J. A. Collins, D. Lizarralde, R. L. Evans, and G. Hirth (2016). High-resolution seismic constraints

on flow dynamics in the oceanic asthenosphere, *Nature* **535,** 1–9, doi: 10.1038/nature18012.

Love, A. E. H. (1927). *A Treatise on the Mathematical Theory of Elasticity*, Fourth Ed., Cambridge University Press, Cambridge, United Kingdom, 643 pp.

Montagner, J. P., and T. Tanimoto (1991). Global upper mantle tomography of seismic velocities and anisotropies, *J. Geophys. Res.* **96,** 20,337–20,351, doi: 10.1029/91JB01890.

Morris, G. B., R. W. Raitt, and G. G. Shor Jr. (1969). Velocity anisotropy and delay-time maps of the mantle near Hawaii, *J. Geophys. Res.* **74,** no. 17, 4300–4316, doi: 10.1029/JB074i017p04300.

Moulik, P., and G. Ekström (2014). An anisotropic shear velocity model of the Earth's mantle using normal modes, body waves, surface waves and long-period waveforms, *Geophys. J. Int.* **199,** 1713–1738, doi: 10.1093/gji/ggu356.

Musgrave, M. J. P. (1970). *Crystal Acoustics; Introduction to the Study of Elastic Waves and Vibrations in Crystals*, Vol. xv, Holden-Day, San Francisco, California, 288 pp.

Nettles, M., and A. M. Dziewonski (2008). Radially anisotropic shear velocity structure of the upper mantle globally and beneath North America, *J. Geophys. Res.* **113,** no. B02303, doi: 10.1029/2006JB004819.

Nishimura, C. E., and D. W. Forsyth (1989). The anisotropic structure of the upper mantle in the Pacific Ocean, *Geophys. J. Roy. Astron. Soc.* **96,** 203–229, doi: 10.1111/j.1365-246X.1989.tb04446.x.

Nye, J. F. (1985). *The Physical Properties of Crystals, Their Representation by Tensors and Matrices*, Oxford Science Press, Oxford, United Kingdom, 329 pp., ISBN: 0-19-851165-5.

Okal, E. A., N. Saloor, S. H. Kirby, and M. Nettles (2018). An implosive component to the source of the deep Sea of Okhotsk earthquake of 24 May 2013: Evidence from radial modes and CMT inversion, *Phys. Earth Planet. Int.* **281,** 68–78, doi: 10.1016/j.pepi.2018.04.007.

Raitt, R. W., G. G. Shor Jr., T. J. G. Francis, and G. B. Morris (1969). Anisotropy of the Pacific upper mantle, *J. Geophys. Res.* **74,** 3095–3109, doi: 10.1029/JB074i012p03095.

Robson, G., K. Barr, and L. Luna (1968). Extension failure: An earthquake mechanism, *Nature* **218,** 28–32, doi: 10.1038/218028a0.

Ross, A., G. R. Foulger, and B. R. Julian (1996). Non-double-couple earthquake mechanisms at The Geysers geothermal area, California, *Geophys. Res. Lett.* **23,** 877–880, doi: 10.1029/96GL00590.

Russell, J. B., J. B. Gaherty, P.-Y. P. Lin, D. Lizarralde, J. A. Collins, G. Hirth, and R. L. Evans (2019). High-resolution constraints on Pacific upper mantle petrofabric inferred from surface-wave anisotropy, *J. Geophys. Res.* **124,** 631–657, doi: 10.1029/2018JB016598.

Stierle, E., M. Bohnhoff, and V. Vavryčuk (2014). Resolution of non-double-couple components in the seismic moment tensor using regional networks—II: Application to aftershocks of the 1999 M_w 7.4 Izmit earthquake, *Geophys. J. Int.* **196,** 1878–1888, doi: 10.1093/gji/ggt503.

Stierle, E., V. Vavryčuk, J. Šílený, and M. Bohnhoff (2014). Resolution of non-double-couple components in the seismic moment tensor using regional networks—I: A synthetic case study, *Geophys. J. Int.* **196,** 1869–1877, doi: 10.1093/gji/ggt502.

Vaišnys, J. R., and C. C. Pilbeam (1976). Deep-earthquake initiation by phase transformation, *J. Geophys. Res.* **81,** 985–988, doi: 10.1029/JB081i005p00985.

Vavryčuk, V. (2001). Inversion for parameters of tensile earthquakes, *J. Geophys. Res.* **106,** 16,339–16,355, doi: 10.1029/2001JB000372.

Vavryčuk, V. (2002). Non-double-couple earthquakes of January 1997 in West Bohemia, Czech Republic: Evidence of tensile faulting, *Geophys. J. Int.* **149,** 364–373, doi: 10.1046/j.1365-246X.2002.01654.x.

Vavryčuk, V. (2004). Inversion for anisotropy from non-double-couple components of moment tensors, *J. Geophys. Res.* **109,** no. B07306, doi: 10.1029/2003JB002926.

Vavryčuk, V. (2005). Focal mechanisms in anisotropic media, *Geophys. J. Int.* **161,** 334–346, doi 10.1111/j.1365-246X.2005.02585.x.

Vavryčuk, V. (2011). Tensile earthquakes: Theory, modeling, and inversion, *J. Geophys. Res.* **116,** no. B12320, doi: 10.1029/2011JB008770.

Vavryčuk, V. (2015). Moment tensor decompositions revisited, *J. Seismol.* **19,** 231–252, doi: 10.1007/s10950-014-9463-y.

Vavryčuk, V., M. Bohnhoff, J. Jechumtálová, P. Kolář, and J. Šílený (2008). Non-double-couple mechanisms of micro-earthquakes induced during the 2000 injection experiment at the KTB site, Germany: A result of tensile faulting or anisotropy of a rock? *Tectonophysics* **456,** 74–93, doi: 10.1016/j.tecto.2007.08.019.

Wiens, D. A., J. J. McGuire, and P. J. Shore (1993). Evidence for transformational faulting from a deep double seismic zone in Tonga, *Nature* **364,** 790–793, doi: 10.1038/364790a0.

Manuscript received 18 December 2019
Published online 5 May 2020